Science of the Total Environment 774 (2021) 145651

Contents lists available at ScienceDirect

Science of the Total Environment

journal homepage: www.elsevier.com/locate/scitotenv

Vegetation structure drives forest phenological recovery after hurricane

Yuan Gong [a,b], Christina L. Staudhammer [b], Gavin Kenney [b], Susanne Wiesner [b,c], Yinlong Zhang [a,*], Gregory Starr [b,*]

[a] Co-Innovation Center for Sustainable Forestry in Southern China, College of Biology and the Environment, Nanjing Forestry University, Nanjing 210037, China
[b] Department of Biological Sciences, The University of Alabama, Tuscaloosa, AL 35487, USA
[c] Department of Biological Systems Engineering, University of Wisconsin-Madison, Madison, WI 53706, USA

HIGHLIGHTS

- Phenological model was parameterized with multi-source data pre- and post-storm.
- Hurricane may have caused an early end to the growing season.
- Forest structure is a primary driver of productivity recovery after hurricane.
- Heterogeneity of site-level leaf area controls the post-storm phenology

GRAPHICAL ABSTRACT

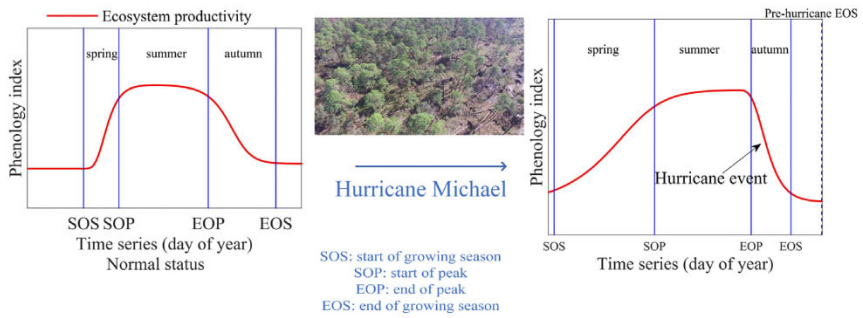

ARTICLE INFO

Article history:
Received 14 October 2020
Received in revised form 5 January 2021
Accepted 31 January 2021
Available online 5 February 2021

Editor: Elena Paoletti

Keywords:
Subtropical forests
Hurricane Michael
Growing season length
Eddy covariance
Phenology model
Longleaf pine

ABSTRACT

Hurricanes affect the structure and function of forests by removing leaf area, reducing biomass, and causing plant mortality. Quantifying the effects of hurricanes on the phenological processes of forests can help to develop a better understanding of the responses of these systems to natural disasters. On October 10, 2018 Hurricane Michael made landfall in the northern Gulf of Mexico causing extensive damage to forests within its path. Using a phenology model, we evaluated the short-term response and recovery of phenological processes of two subtropical forests that were affected by the storm. Our results suggest that the hurricane accelerated senescence in autumn following the storm, leading to a shorter growing season. The response was dependent on the structure of the forest prior to the storm and the degree of damage; the forest with a taller canopy had greater damage, and the recovery period was prolonged compared to the forest with a shorter canopy. In the summer of the first year following the hurricane, ecosystem physiological function began to return to pre-hurricane levels which corresponded to a recovery in growing season length. The functional diversity in the understory may have aided recovery of post-hurricane spring phenology. While summer phenology was synchronized with the rate of vegetation coverage and mainly driven by increase in canopy leaf area, these forests have not completely recovered during the study. As extreme weather events and disasters induced by global climate change may become more frequent, our research can provide a reference for post-disaster forest management practices which can be adapted to local conditions and contribute to restoration efforts.

1. Introduction

Rising ocean temperatures caused by global warming may lead to increased intensity of hurricanes (Chen, 2019). Hurricanes can cause varying degrees of structural and functional damage to terrestrial

* Corresponding authors.
E-mail addresses: zylnjfu@gmail.com (Y. Zhang), gstarr@ua.edu (G. Starr).

https://doi.org/10.1016/j.scitotenv.2021.145651
0048-9697/

ecosystems, especially in forests with tall canopies (Harrington et al., 1997; Hogan et al., 2020). These wind disturbances directly affect forest ecosystem function, which in turn impacts ecosystem services (e.g., carbon sequestration, food and water supply or nesting sites, Renton et al., 2018; Hogan et al., 2020).

Understanding forest phenological cycles after a hurricane can contribute to more accurate assessments of the impact of natural disasters on their functions, more reasonable post-disaster management strategies, and a better understanding of forest responses to extreme weather (Enquist et al., 2014). Studies have indicated that forest carbon cycles are directly affected by the phenology of the ecosystem, and a longer growing season can promote greater carbon uptake and faster recovery (Gonsamo et al., 2015; Gong et al., 2020). Therefore, quantifying forest phenological changes and recovery from hurricanes can lead to a better understanding of ecosystem physiological functions in response to disturbances associated with global climate change (Gong et al., 2020).

Research on forest phenology has mainly focused on growing season length, leaf development (e.g., leaf-out/on, mature, and leaf-off/dormancy) (Enquist et al., 2014), and the response of phenological processes to weather and disturbances at different ecological scales (Gonsamo et al., 2015; Gong et al., 2020). These studies mainly relied on remote sensing (RS)-based and/or ground-based time series of vegetation indices (Gonsamo et al., 2015; Zhang et al., 2003). Patterns of plant community growth have been simulated through statistical or physiological models, and ecosystem-scale phenological nodes, including: the start of growing season (SOS), end of growing season (EOS), and the length of growing season (LOS) (Zhang et al., 2003; Gu et al., 2003). Currently, the quantification of forest phenological characteristics using this approach has become an important research field and has been applied to various ecosystems across different climatic zones (Gonsamo et al., 2013, 2015; Gong et al., 2019). However, these studies usually link phenological process of forests with conventional meteorological data (air temperature, precipitation, radiation, etc.) (Niu et al., 2013; Gonsamo et al., 2015), and rarely involve natural disasters or extreme weather events. Moreover, previous work indicates that the specificity of ecological memory and ecosystem components across the landscape may lead to different response mechanisms, effect sizes, and variability in subsequent recovery process with hurricanes (Hogan et al., 2020). In addition, since the availability of ground observations is often limited by extreme weather events, the response of ecosystem phenological processes to disturbances has not been well-studied. Therefore, quantifying the dynamics of the growing season using forest phenological data to characterize extreme events may provide a better understanding of how the system recovers after natural disasters (Angulo-Sandoval et al., 2004; Renton et al., 2018).

On October 10, 2018, Hurricane Michael made landfall in the northern Gulf of Mexico. This area is heavily forested, including several important species of pines (*Pinus* spp.), which received a high degree of damage. Despite this, there have been no prior studies detailing the impact of the hurricane on forest phenological processes and/or post-storm recovery in the region. This study provides insight into the phenological characteristics of two longleaf pine (*Pinus palustris*) forests with differing soil water holding capacity (xeric and mesic), which had significant structural damage associated with the hurricane. Due to site-specific soil properties, the xeric site, which is subject to chronic water limitation (Starr et al., 2016), has a unique structure, i.e., shorter forest canopy, sparse midstory and understory communities (Kirkman et al., 2001). Such forest structure may be more resistant to physical damage caused by hurricane-induced wind disturbance in comparison to the mesic site, which has a taller canopy and higher basal area (Wiesner et al., 2019).

For each site, we used three years (the year prior, year of, and year after Hurricane Michael) of eddy covariance (EC) CO_2 fluxes to parameterize the phenological model developed by Gu et al. (2003), as well as remote sensing (RS) and LiDAR data of pre- and post-storm forest canopy height as indicators of hurricane-induced forest damage. We addressed the following two hypotheses: (1) The hurricane will accelerate the autumn senescence by inducing early EOS and shorter LOS for the year of the storm, with the xeric site recovering faster in comparison to the mesic due to ecological memory associated with water limitations, (2) Ecosystem-scale leaf area index (LAI) and enhanced vegetation index (EVI) will affect site-level phenological processes, i.e., rapid LAI and EVI recovery after hurricane will be associated with recovery during spring green-up.

2. Materials and methods

2.1. Study sites

Our two research sites represent the ends of an edaphic gradient and are located at the Jones Center at Ichauway in southwestern Georgia, USA. The center is a 11,000 ha^2 long-leaf pine reserve (31.22° N, 84.47° W; Fig. 1), which has a subtropical humid climate (Wiesner et al., 2018, 2019). The long-term average annual precipitation of the study area is 1310 mm. Temperatures range from 22 °C to 33 °C during summer and from 3 °C to 16 °C during winter (NCDC, 2011). We utilized data from two EC flux towers equipped with CO_2/H_2O infrared gas analyzers, a micro-meteorological observation system and data logger (Wiesner et al., 2020). Due to the different soil water availability, the two EC sites have differences in forest structure and composition (Table 1; Kirkman et al., 2001; Starr et al., 2015). The mesic site lies on somewhat poorly drained sandy loam over sandy clay loam and clay textured soils (Goebel et al., 1997). The xeric site lies on well-drained deep sandy soils with no argillic horizon (Goebel et al., 1997). This well-drained soil leads to this difference is water soil holding capacity. The two sites are situated within 5 km of each other, with an elevation above sea level of 65 m for the mesic site, and 60 m for the xeric site. In the flux footprint area of the two EC flux towers, longleaf pine trees (*Pinus palustris* Mill.) are the dominant tree species, averaging ~100-years in age, and understory vegetation includes shrubs such as *Diospyros virginiana* L. and *Aristida stricta* Michx (Kirkman et al., 2013; Wiesner et al., 2020).

Longleaf pine ecosystems have evolved with frequent fire (every 1–3 years; Christensen, 1981); when fire is suppressed for as little as 4 years, the ecosystem loses biodiversity and its structure and function are altered (Way, 2006). Both sites are on a 2-year burn cycle and are burned in odd years during the winter when many understory plants are dormant. The fires are set using backing fires on the downwind side of the management unit, moving the fire away from a downwind firebreak. Strip head fires are then set perpendicular to the wind, starting on the downwind end of the unit and moving upwind. This practice promotes low intensity fires, with limited flame lengths and damage to the overstory (Starr et al., 2015).

2.2. Parametric phenology model of plant community photosynthesis

This study used a nine-parameter phenology model employing gross primary production (GPP) (Gu et al., 2003, 2009; Eq. (1)) to analyze the dynamic changes in phenology at each site from 2017 through 2019, and to determine the potential impact of the hurricane on the phenology of the two forests. This GPP-based phenology model was originally developed utilizing inter-annual daily maximum GPP ($\mu mol\ CO_2\ m^{-2}\ s^{-1}$) obtained from 30-min EC measurements to quantify phenological phases (Gu et al., 2003, 2009). However, although there is significant seasonal variation in GPP derived from 30-min EC data (Whelan et al., 2013), models of daily maximum GPP do not yield ecologically meaningful estimates of phenology (Gong et al., in review). Therefore, the phenology model was parametrized with daily cumulative GPP ($g\ C\ m^{-2}\ d^{-1}$) to represent the seasonal pattern of the canopy and understory activity following Yang and Noormets (2020).

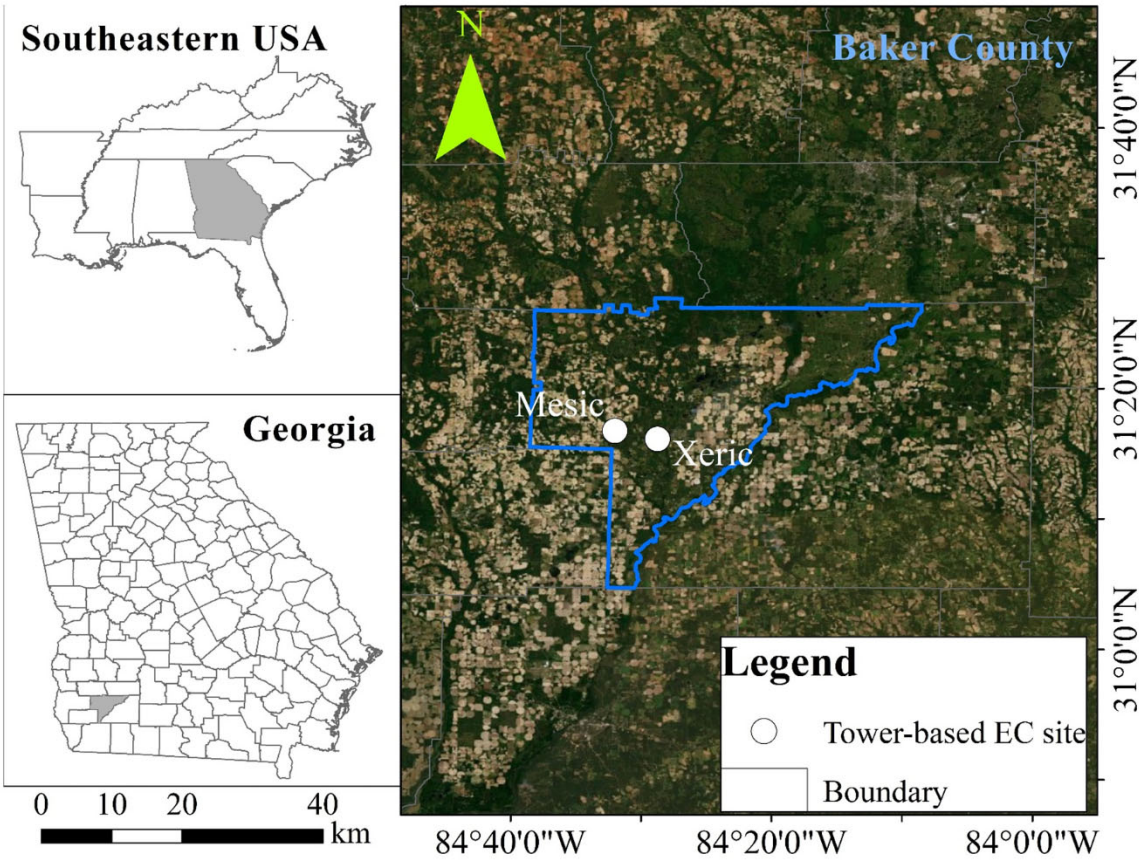

Fig. 1. Geographical locations of two tower-based longleaf pine forest EC sites inside the JCI. USA: United States of America, county-level administrative boundary data was obtained from: USGS National Boundary Dataset (NBD, https://www.usgs.gov/), the geographic coordinate system of these map is GCS_WGS_1984 and processed using ArcGIS version 10.2 (Environmental Systems Research Institute, Redlands, CA, USA).

$$A(t) = y_0 + \frac{a_1}{\left[1 + exp\left(-\frac{t-t_{01}}{b_1}\right)^{c_1}\right]} - \frac{a_2}{\left[1 + exp\left(-\frac{t-t_{02}}{b_2}\right)^{c_2}\right]} \quad (1)$$

$$k(t) = \frac{dA(t)}{dt} = \frac{a_1 c_1}{b_1} \frac{exp\left(-\frac{t-t_{01}}{b_1}\right)}{\left[1 + exp\left(-\frac{t-t_{01}}{b_1}\right)\right]^{1+c_1}} - \frac{a_2 c_2}{b_2} \frac{exp\left(-\frac{t-t_{02}}{b_2}\right)}{\left[1 + exp\left(-\frac{t-t_{02}}{b_2}\right)\right]^{1+c_2}} \quad (2)$$

Table 1
Stand characteristics and mean environmental variables (±1 S.D.) for the mesic and xeric longleaf pine study sites at the Joseph W. Jones Ecological Research Center in Georgia, USA. BA = basal area, DBH = diameter at breast height, LAI = leaf area index, and EVI = enhanced vegetation index.

Stand characteristic	Mesic	Xeric
B_A all tree spp. (m^2 ha^{-1})	18.4 (±1.7)	11.1 (±2.9)
B_A *P. palustris* (m^2 ha^{-1})	17.4 (±2.1)	8.2 (±3.8)
DBH (cm)	25.7 (±15.2)	18.1 (±13.8)
Proportion of oak trees (%)	8.0	22.0
Wiregrass abundance (%)	28	24
Woody plant abundance (%)	12	10
Soil drainage	Poorly drained	Excessively well-drained
Water holding capacity (cm per m soil in upper 3 m)	40	18
$LAI_{MODIS,\ growing\ season}$ (m^2/m^2)	2.55 (±0.7)	2.27 (±0.6)
$LAI_{MODIS,\ non\text{-}growing\ season}$ (m^2/m^2)	1.34 (±0.46)	1.06 (±0.43)
$EVI_{MODIS,\ growing\ season}$	0.418 (±0.046)	0.412 (±0.049)
$EVI_{MODIS,\ non\text{-}growing\ season}$	0.314 (±0.03)	0.284 (±0.03)

where: $A(t)$ is daily cumulative GPP (g C m^{-2} d^{-1}) at day t ($t = 1, \ldots, 365$) and $k(t)$ is the GPP growth rate/slope function (g C m^{-2} d^{-1} d^{-1}), estimated by site and year; a_1, a_2, b_1, b_2, c_1, c_2, t_{01}, t_{02}, and y_0 are empirical fitting parameters estimated for each site and year. Measured daily cumulative GPP data were used to parameterize $A(t)$, which was then used in the $k(t)$ function to calculate the growth rate of GPP (Gu et al., 2009; Eq. (2)). Then, phenological parameters describing the start of growing season (SOS), end of growing season (EOS), start of peak (SOP), day of peak (DOP) and end of peak (EOP; Fig. 2), etc. were defined as the Julian day derived from the recovery and senescence lines following Gu et al. (2009) (Fig. 2). This phenology model was coded and visualized in MATLAB R2014b (MathWorks Inc., Natick, USA).

2.3. Response of spring recovery phenology to hurricane-induced disturbance

Spring phenology in the first year following the hurricane is important in characterizing post-storm ecosystem recovery (Li et al., 2007). Here, spring is defined as those days between SOS and SOP (Figs. 2, 3). The arithmetic midpoint between SOS and SOP is defined as the midpoint of spring (MOS). In this subtropical study landscape, the response duration of spring plant community development to environmental variables and disturbance has been characterized on a monthly scale

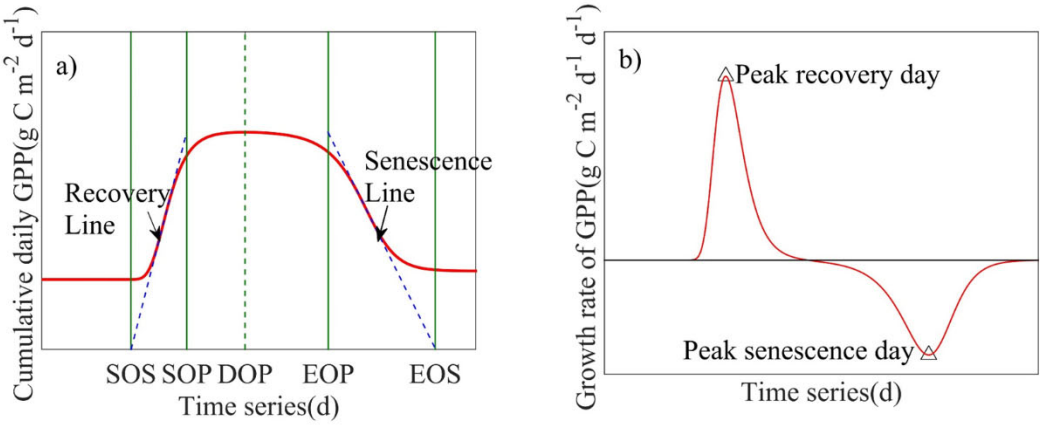

Fig. 2. Schematic diagram of estimated phenological events derived from daily cumulative GPP (gross primary production) over an entire year (Julian Day 1 through 365). (a) $A(t)$ is the fitted red curve where spring is defined as those days between start of the season (SOS) and start of peak (SOP), summer as the days between SOP and end of peak (EOP), and autumn as EOP through end of growing season (EOS). DOP is the day of peak. (Winter is the period between EOS and the following year's SOS.) (b) $k(t)$ is the fitted red curve, black triangle represents the extreme values of the daily change of modeled daily GPP, defined by Gu et al. (2009).

(Whelan et al., 2013). We therefore defined the two weeks before MOS as the middle of spring buffer zone. To characterize post-hurricane-specific spring phenology, the time period during spring before this buffer zone was defined as early spring, and the time period during spring following the buffer zone was defined as late spring (Fig. 3).

2.4. Net ecosystem exchange CO_2 using Eddy covariance

EC data were used to parameterize the phenological model (net ecosystem exchange of CO_2, NEE). The open-path EC system collected data at 10 Hz (Starr et al., 2015, 2016) using a LI-COR CO_2/H_2O infrared gas analyzers (Li-7500, LI-COR, Lincoln, NE, USA) accompanied by three-dimensional high precision sonic anemometers (CSAT-3, Campbell Scientific Instruments, Logan, UT, USA). Each EC measurement system was installed approximately 4 m above mean canopy height (Starr et al., 2015, 2016). The tower heights were 34.4 and 34.9 m above ground, for the mesic and xeric sites, respectively, resulting in upwind flux source areas that extend a radius of approximately 600 m from each tower (Starr et al., 2015).

Meteorological data, including photosynthetically active radiation (PAR; LI-190, LI-COR Inc., Lincoln, NE, USA), global radiation (LI-200SZ, LI-COR Inc., Lincoln, NE, USA), net radiation (NR01, Hukseflux Thermal Sensors, Delft, The Netherlands), precipitation (TE525 Tipping Bucket Rain Gauge, Texas Electronics, Dallas, TX, USA), and air temperature and relative humidity (HMP45C, Campbell Scientific Instruments, Logan, UT, USA) were collected above the canopy and stored on a CR-5000 dataloggers (Campbell Scientific Instruments, Logan, UT, USA).

2.5. Gross primary production estimations from EC-measured NEE

This study used CO_2 flux data collected from two sites from January 1, 2017 through December 31, 2019, which included one calendar year prior to the hurricane, the year which included Hurricane Michael (October 10, 2018), and one year of following the hurricane. Flux data was processed with the EdiRe software (v.1.4.3.1184; Starr et al., 2015, 2016) to calculate CO_2 flux at 30-minute intervals, using a coordinate rotation, frequency response correction, WPL density correction and spectral attenuation. QA/QC of the CO_2 flux data was also maintained by filtering out data that did not pass plausibility tests (i.e., NEE < -30 and NEE > 30 μmol CO_2 m^{-2} s^{-1}), stationarity criteria, and integral turbulent statistics (Starr et al., 2015).

Missing and disqualified half-hourly CO_2 flux data were gap-filled using separate functions for NEE during daytime and nighttime. When photosynthetically active radiation (PAR) was ≥10 μmol m^{-2} s^{-1},

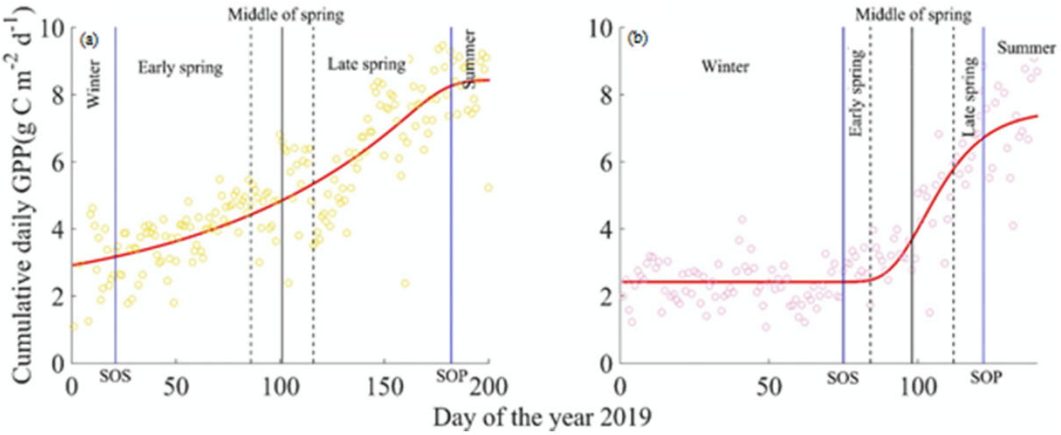

Fig. 3. Post-hurricane spring phenological phase derived from daily GPP (gross primary production) by site in 2019: (a) yellow circles in mesic site, and (b) pink circles in xeric site. The red curve represents the modeled GPP using $A(t)$, black vertical solid line represents MOS (midpoint of spring, DOY), and the dashed black lines on both sides represent the two-week buffer (middle of spring).

daytime NEE data were gap-filled using a Michaelis-Menten approach, and when PAR was <10 μmol m^{-2} s^{-1}, nighttime NEE data were gap-filled using a modification of the Lloyd and Taylor (1994) approach, both on a monthly basis (Whelan et al., 2013; Wiesner et al., 2018). Where too few observations were available to produce stable and biologically reasonable parameter estimates, annual equations were used to gap-fill daytime and nighttime NEE data by site. Half hourly fluxes of NEE in μmol CO_2 m^{-2} s^{-1} were used to calculate gross primary production (GPP) and ecosystem respiration (Re, Starr et al., 2015, 2016) as follows:

$$Re = GPP + NEE \quad (3)$$

Due to equipment and power outages sustained from the hurricane, EC observations were not available during and immediately after the hurricane. Therefore, we used a linear regression approach to estimate these data with RS-derived GPP (g C m^{-2} d^{-1}) during 10/18/2018 through 1/7/2019, and 10/4/2018 through 10/28/2018 at the mesic and xeric sites, respectively (detailed data description for RS is found in Section 2.6). EC-derived GPP from 2017 to 2018 was first summarized to the 8-day periods corresponding to the MODIS measurement dates. Using the R function lm with RStudio (R Core Team, 2013), EC-derived GPP was best predicted as a function of the current period MODIS GPP, as well as the previous and following 8-day periods. The resulting models explained 78% and 74% of the variation, respectively, in the mesic and xeric EC-derived GPP.

2.6. Remote sensing vegetation indices

LAI and EVI are important biological indicators used to assess the vegetative growth and in some cases vegetation status following hurricanes (Li et al., 2007; Gong et al., 2019). To quantify the site-level forest damage caused by hurricane and post-hurricane vegetation recovery, we obtained 2017–2019 500-m spatial resolution and 8-day interval LAI and EVI data from the NASA Moderate Resolution Imaging Spectroradiometer (MODIS, https://ladsweb.modaps.eosdis.nasa.gov/) Vegetation Index Products (MOD15AH2) for the two study sites (Appendix A, Fig. A1).

To gap-fill missing EC measurements due to hurricane damage that left the tower non-operational, we obtained 500-m spatial resolution and 8-day interval GPP data from 2017 to January 2019 from MODIS Vegetation Index products (MOD17AH2). MODIS-derived LAI and GPP data were processed with the MODIS Reprojection Tool (MRT) using ArcGIS (Version 10.2; ESRI) for projection correction, image cropping, and raster calculation. Since the EC flux source area can be extended up to 600 m from the towers (Wiesner et al., 2018, 2019), MODIS-derived GPP, LAI and EVI were average values within 600 m radius circles centered at each EC sites.

2.7. Forest canopy height measurements using Light Detection and Ranging (LiDAR)

One-meter resolution airborne LiDAR data were acquired from the National Ecological Observatory Network (NEON, 2020). LiDAR scans have been performed annually in September since 2016, with the most recent flight occurring in early September 2019. We obtained LiDAR data from 2018 and 2019 through NEON's Airborne Observation Platform (AOP), which consists of an imaging spectrometer, a waveform LiDAR instrument, and a high definition digital camera. The instruments are installed in a Dehavilland DHC-6 Twin Otter aircraft which flies at 1000–2000 m above ground level at 100 knots. The waveform instrument produces a laser with normal pulse repetition frequency at ~100 kHz, which reflects off a surface and returns to the instrument, and a signal detection algorithm calculates the X, Y, and Z position alongside the signal intensity. Extensive information about the data processing, algorithms, and uncertainty, which can occur due to sensor error or variability in terrain reflectivity and vegetation type, can be found in the NEON technical documentation (Krausse and Goulden, 2015).

The LiDAR point cloud data was used by NEON to create a Canopy Height Model (CHM, https://www.neonscience.org/create-chm-rasters-r). Point cloud data for each site in 2019 (post-hurricane) was compared to that of 2018 (pre-hurricane) to measure the changes in canopy height pre- versus post-storm. ArcGIS Pro (Version 2.4.1; ESRI) was used to measure changes in canopy height within the 500-meter radius of each EC flux tower using geoprocessing tools available in the program.

2.8. Statistical analysis

The fit of the phenology model was verified by examining the adjusted coefficient of determination (R^2). We judged the model to have good fit when $R^2 > 0.8$ following Yang and Noormets (2020).

`Models were formulated to test hypotheses using the 8-day MODIS LAI and EVI, and EC-derived GPP data. Because there is the potential for high amounts of autocorrelation among observations taken in adjacent time periods, we formulated generalized least square (GLS) models, specifically accounting for this correlation with an autoregressive (AR(1)) structure. For these analyses we used the function gls in package *nlme* (Pinheiro et al., 2014) in R and RStudio (R Core Team, 2013). To test the hypothesis that hurricane significantly impacted LAI and EVI, we estimated models as a function of site and month, with an interactive effect for hurricane pre- versus post-storm. To test the hypothesis that LAI and EVI impacted ecosystem phenological processes, we modeled GPP as a function of LAI and site, as well as their interactive effects with hurricane (pre- versus post-storm). Least square mean predicted values by site and pre- versus post-hurricane were generated with the R package em*means* (Lenth, 2016).

3. Results

3.1. Effects of Hurricane Michael on forest canopy height and LAI

RS-derived LAI in the mesic site was 15%–30% lower in the month immediately post-storm, with the maximum differences occurring in mid-December, whereas the xeric site experienced less of a drop (Fig. 4a). By February, monthly LAI recovered to pre-hurricane levels; however, LAI at the two sites from March to June was lower than the pre-hurricane level (by 6%–40%) due to prescribed fires that were conducted in March of 2019; monthly LAI of the mesic site recovered to its pre-hurricane level in July, and the xeric site recovered to its pre-hurricane level in September (Fig. 4a). For EVI, there was almost no discernible change in the mesic site pre- versus post-hurricane October–December, while there was a noticeable drop in the xeric site (Fig. 4b). In January–March, however, the EVI at both sites were higher post-storm versus pre-storm. While the xeric site appeared to recover from March onward post-storm, the mesic site EVI dropped well below normal through July, and only recovered after this period (Fig. 4b). The GLS model indicated that LAI significantly differed by site and pre- versus post-hurricane. However, these effects did not significantly interact, i.e., site responses to hurricane were not significantly different ($P = 0.89$; Appendix A, Table A1). Pre- versus post-hurricane, LAI differences depended on month and there was a significant difference in March and June values of LAI (Fig. 4a). GLS models of EVI, on the other hand, did not indicate significant differences pre-versus post-storm ($p = 0.16$), or among sites ($p = 0.12$). Analyses of LiDAR data revealed that there was a reduction in average canopy height of 1.30 and 0.28 m at the mesic and xeric sites, respectively (Fig. 5).

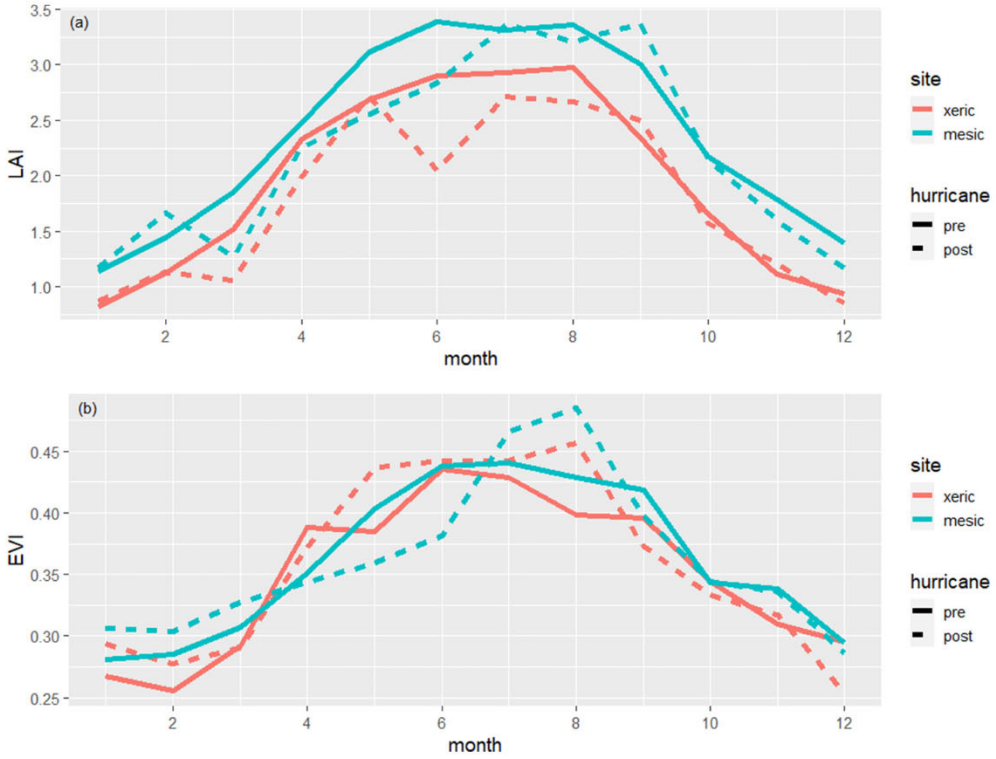

Fig. 4. Least square mean predicted values of RS-derived (a) leaf area index (LAI) and (b) enhanced vegetation index (EVI) by site, pre- (1/1/2017–10/8/2018) versus post-hurricane (10/16/2018–12/30/2019). Colors indicate the site (xeric versus mesic), solid lines are pre-storm whereas dotted lines are post-storm.

3.2. Hurricane-induced variation in GPP-derived phenological processes at site-level

The phenology model was used to evaluate phenological changes in physiological function and photosynthetic capacity of plant communities before and after the hurricane by site (Appendix A, Figs. A2, A3). All corresponding R^2 were greater than 0.8, indicating good model fit. To account for the two-year cycle of needle replacement and inter-annual climate differences, we compared the acquired phenological parameters of each year with the previous year at each site.

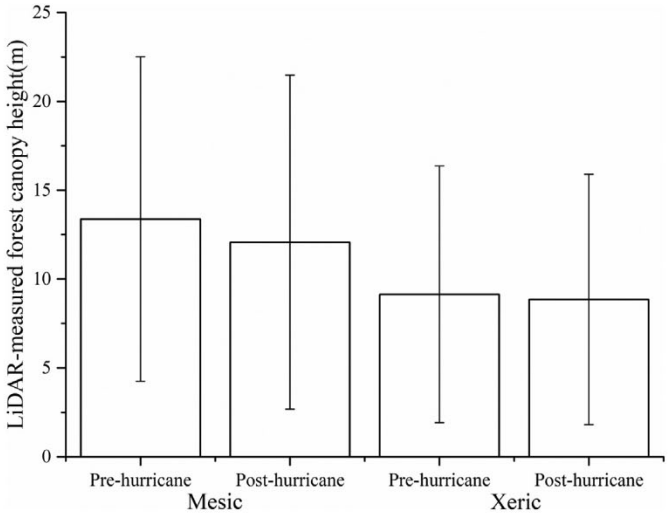

Fig. 5. LiDAR-derived forest canopy height for the two study sites (±1 S.D.); pre-storm measured September 2018 and post-storm measured September 2019. (Year 2017 data were not available due to an AOP flight line error.)

For the mesic site, the 2017 autumn-related phenological parameters EOS and LOS were at DOY 365 and 364, respectively, and autumn length was 127 days. Prior to Hurricane Michael in 2018, spring and summer lengths were 134 and 129 days respectively. The immediate impact of the hurricane on the phenological processes was reflected in 2018 autumn phenology and led to an early EOS (41 days early) with a LOS of 316 days (48 days short). Moreover, 2018 autumn length was shortened by 74 days (to 53 days) compared with 2017. After the end of winter in 2018, the ecosystem entered the recovery period in late January 2019. Compared with 2018, the length of spring in 2019 was extended to 161 days with a MOS at DOY 101 (Fig. 3), summer length was shortened to 70 days, and autumn length was 81 days. In 2019, 223 days after the hurricane impact, the summer photosynthetic capacity of plants at the mesic site recovered to its pre-hurricane peak level (SOP; Appendix A, Fig. A3).

In 2017, the xeric site autumn-related phenological parameters EOS and LOS were at DOY 365 and 357, respectively, and autumn length was 131 days. The lengths of spring and summer in 2018 (prior to Hurricane Michael) were normal: 50 and 144 days, respectively. The autumn GPP declined rapidly after hurricane impact in 2018, which was associated with the growing season end on DOY 332 (33 days early) with a LOS of 262 days (95 days short). Moreover, 2018 autumn length was shortened by 63 days (to 68 days) compared with 2017 (Appendix A, Fig. A3). In contrast to the mesic site, the 2019 spring recovery period of the xeric site was not extended by hurricane (47 days), with a MOS at DOY 98 (Fig. 3). Thus, after MOS, subsequent ecosystem phenological processes were not affected by the hurricane (Fig. 3), where summer and autumn had normal lengths (119 and 90 day, respectively) (Appendix A, Fig. A3). The xeric site recovered more quickly to its pre-hurricane peak photosynthetic capacity (reaching SOP 156 days after the hurricane impact; Appendix A, Fig. A3).

Overall, the impact of the hurricane on the xeric site's autumn phenology in 2018 was less than that of the mesic site (Appendix A, Figs. A2–A3); although the EOS of both sites appeared earlier in 2018

than 2017, EOS of mesic site was more advanced (41 days early for mesic, 33 days early for xeric). In addition, the spring recovery period of the xeric site in 2019 did not extend as it did in the mesic site. This result suggests that the hurricane has had more impact on the GPP-derived phenological processes at the mesic versus the xeric site (Appendix A, Figs. A2–A3).

3.3. Relationship between LAI and spring productivity net recovery after hurricane

Results from the GLS model indicated that LAI was a strong and significant driver of GPP, and its effects on GPP were significantly different pre- versus post-hurricane. However, with LAI in the model (which was significantly different by site; $P < 0.0001$), there were no significant differences in GPP by site. GLS models of GPP with EVI as a predictor indicated no significant ($p > 0.05$) effects of EVI on GPP, nor with its interaction with hurricane or site. To better understand the relationship between plant community phenology and LAI pattern after hurricane in 2019, we compared the growth rate of the fitted LAI curve (Appendix A, Fig. A4) and the growth rate of the fitted GPP curves in spring, summer, and autumn by site (Fig. 4). We found that the 2019 LAI curve of the mesic site was similar to that of the GPP curve, with a longer spring recovery period; however, the xeric site's LAI curve indicated a relatively shorter spring recovery period (Appendix A, Fig. A4). The mesic site's longer spring length after hurricane was due in part to its shallower-sloped LAI curve during the spring green-up period (0.012 $m^2\ m^{-2}\ d^{-1}$), which was lower than that of the xeric site (0.017 $m^2\ m^{-2}\ d^{-1}$).

For the mesic site, in 2019 summer and autumn, the increase in LAI was consistent with increases in GPP (positive correlation). However, there was a clear "turning point" in the spring phenology; we found that the date of LAI's spring maximum occurred at DOY 108 (mid-spring), earlier than the date of GPP's spring maximum (DOY 160, late spring) (Fig. 3). This resulted in a significant positive correlation between GPP and LAI between the SOS until DOY 108, then this correlation became negative during DOY 109–160. This may be attributed to the March prescribed fire that removed understory vegetation, as prescribed fire has been found to have an effect on the ecosystem for ~30–60 days following fire (Starr et al., 2015).

Patterns at the xeric site were similar to that of the mesic site, as the recovery rates of GPP and LAI in 2019 summer and autumn were positively correlated. The "turning point" also appeared in the spring, with the date of maximum recovery rate of LAI (DOY 81, in early spring) earlier than the date of maximum recovery rate of GPP (DOY 102, in middle of spring) (Fig. 3).

By comparison, we found that LAI and GPP at the xeric site were faster to reach the maximum recovery rate in 2019 spring, and the lag between the DOY of the GPP maximum recovery rate and LAI maximum recovery rate was 21 days shorter than that of the mesic site (52 days). In addition, the maximum recovery rate of GPP and LAI in the xeric site in spring (0.16 g C $m^{-2}\ d^{-1}\ d^{-1}$ and 0.019 $m^2\ m^{-2}\ d^{-1}$, respectively) was also higher than that of the mesic site (0.05 g C $m^{-2}\ d^{-1}\ d^{-1}$ and 0.015 $m^2\ m^{-2}\ d^{-1}$, respectively).

4. Discussion

Our results showed that the two sites were affected and responded differently to the hurricane, with a greater reduction in leaf area and forest canopy height at the mesic site than the xeric site (Figs. 4, 5). The differences in damage can be linked to the mesic site having greater density and taller trees in the canopy, which has been shown to have an influence on storm damage (Johnsen et al., 2009; Bigelow et al., 2020; Hogan et al., 2020). This increased damage led to shifts in ecosystem phenological process (Li et al., 2007; Angulo-Sandoval et al., 2004), which was represented by the advance of EOS during the storm year, and then a shortened LOS. The spring recovery period in the first year following the hurricane was extended in proportion to the degree of forest structure damage by site. Moreover, the rate of plant growth and recovery after hurricane lagged that of GPP in both sites. We attributed this to increased light reaching the forest floor; this may have increased surface temperatures, causing higher ecosystem respiration which would have influenced the calculation of GPP (Kenney et al., unpublished data).

4.1. Impact of hurricane damage on site-level phenological processes

The hurricane occurred in the fall of 2018 which coincided with seasonal leaf senescence; however, the evergreen-dominant canopy showed moderate rates of mortality and there was an overall loss of LAI and a slight decline in EVI (Ostertag et al., 2005). Moreover, continuously heavy rainfall associated with the storm may have led to lower light availability, which reduced photosynthetic activity at the sites (Tanner et al., 1991; Zhang et al., 2018). As a result, autumn senescence was accelerated, which ended the growing season early and shortened the overall growing season. The seasonal productivity of subtropical vegetation is expected to be symmetric under conditions without disturbance (Zhang et al., 2020; Zhou, 2019), i.e., the spring phenology of the "slow-in" form corresponds to the autumn phenology of the "slow-out" form (Zhou, 2019); however, the disturbance caused the "rapid-out" autumn phenology form at the site-level which contributed to the reduction in growing season length which was also seen in the MODIS EVI measurements (Fig. 4b).

Eight months after the hurricane, ecosystem physiological functions returned to pre-hurricane rates which were also confirmed by EVI, in agreement with the findings of Herbert et al. (1999). However, the mesic site, which experienced greater damage, had a longer spring recovery period. This delayed the SOP (Fig. 3), but since the end date of the summer was not affected, autumn phenology was unaffected. Therefore, we observed that the impact of Hurricane Michael on ecosystem-scale phenology during the following year was mainly reflected in the length of spring and summer (i.e., the timing of SOP, Fig. 2). We predict that during the second year after hurricane (2020), the ecosystem-scale phenological processes of these longleaf pine forests will completely recover from the impact of the storm (Appendix A, Figs. A5–A6).

4.2. Relationship between vegetation development and spring phenology after hurricane

Forest physiological function (photosynthesis etc.) is related to leaf development, which may result in stronger carbon uptake (Li et al., 2018). We observed that spring phenology and ecosystem function were separated into two phases after the hurricane. During the early and mid-spring, the recovery and leaf out rate reached their peak levels (Fig. 3), and productivity also increased with this acceleration of plant growth. After the mid-spring, leaf development began to slow, but ecosystem productivity still increased. This could be attributed to the fact that during needle expansion and understory green up there is an increase in ecosystem respiration in forests (Lindroth et al., 2008). As leaf development declines so do respiration rates, leading to greater carbon sequestration by the ecosystem.

LAI is an important variable that affects the exchange of CO_2 between biosphere and atmosphere (Bonan, 1993; Gonsamo et al., 2012). The mesic site has more understory vegetation (Kirkman et al., 2013; Wiesner et al., 2018), and in the early spring of 2019 (DOY 8 through 87; Fig. 3), the growth and recovery of this understory was likely the source of increasing leaf area, as was found by Badeck et al. (2004). Since the forest canopy had not recovered from the damage caused by hurricane, the understory had greater radiation inputs to aid in maximizing light use efficiency (Ma et al., 2020), which is related to canopy gap fraction and shade patterns (Rosati et al., 2020; Yun et al., 2013; Angulo-Sandoval et al., 2004).

However, during the middle of spring 2019 (DOY 88 through 115; Fig. 3), the air temperature reached optimal levels for growth, leading to post-hurricane recovery. During this period, we observed that LAI and ecosystem greenness reached their peak (Fig. 6). This again shifted what light reached the understory vegetation, which may have limited photosynthetically active radiation (PAR) that could drive understory photosynthesis (Drever and Lertzman, 2003; McGuire et al., 2001; Kenney et al., in review).

At the xeric site, the plant community is dominated by evergreen longleaf pine (Wiesner et al., 2018), such that the ecosystem-scale LAI before early spring is mainly associated with the canopy (Badeck et al., 2004). But the low air temperature in winter and early spring (DOY 1 through 75) reduces photosynthetic capacity (Starr et al., 2015). During the early and middle part of spring (DOY 75 through 112), increasing air temperature and LAI contributed to rising photosynthesis, which was similar to pre-storm rates (Whelan et al., 2013). This led to rapid increase in GPP, similar to that of spring phenology patterns in temperate forests which are controlled by air temperature (Niu et al., 2013; Gong and Zhang, 2020). In addition, ecological memory at the xeric site may have aided in accelerating recovery of the start of the growing season in 2019 due to the system's chronic water limitation that has led to the development of a shorter canopy with lower basal area (Starr et al., 2016; Hogan et al., 2020; Chambers et al., 2007).

In summary, our results support the idea that the phenological response of longleaf pine ecosystems is delayed after hurricane due to leaf loss and tree mortality (Figs. 4, 5), such that the development of plant community productivity and leaf greenness are not synchronized during the spring phenophase, in agreement with Kong et al. (2020). Past research has found that the early spring recovery rate of subtropical understory vegetation without light limitation is significantly faster than that of the canopy (Ma et al., 2020). The length of this lag is related to the cumulative demand for light, heat, and water resources of the plant community's site-level photosynthesis during the plant green-up phase (Kong et al., 2020). Utilization efficiency of these resources for plant growth will also affect the lag process, sensitivity of productivity to environmental variables, and both the timing of the start of the growing season and its overall length (Landsberg and Waring, 1997; Badeck et al., 2004; Whelan et al., 2013).

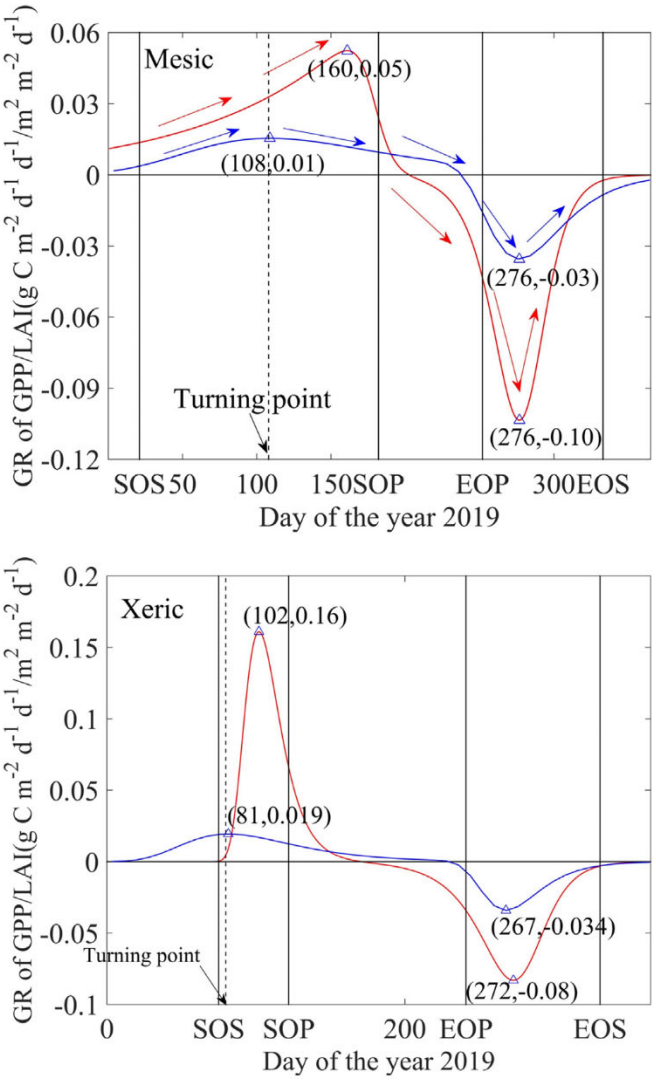

Fig. 6. Growth rate (GR) of modeled GPP (gross primary production; red curve) and LAI (leaf area index; blue curve) after hurricane by site. Blue triangles indicate extreme values. SOS (DOY of start of growing season), SOP (DOY of start of peak), EOP (DOY of end of peak), and EOS (DOY of end of growing season).

4.3. Scaling the response of land surface phenology to disturbance

Due to the heterogeneity of the longleaf ecosystem, responses to extreme weather events vary from stand to stand, and from the stand- to the landscape-scale (Hogan et al., 2020). Our observations at the ecosystem-scale show that plant community differences (forest characteristics and understory components) significantly affect the ecosystem's response to hurricanes from the perspective of resistance and resilience to disturbances (Hogan et al., 2020). Moreover, remotely sensed observations of LAI are consistent with our observed GEE-based post-hurricane ecosystem phenological process. This may indicate that remote sensing has considerable potential in predicting landscape and regional-scale land surface phenology in response to extreme weather events when ground observations are lacking. More generally, terrestrial ecosystems with higher levels of resistance will exhibit reduced immediate damage to physical structures caused by extreme weather events, while those with higher resilience to disturbances will accelerate the restoration of their ecosystem physiological functions after damage to their physical structures. In the process of ecosystem recovery after disturbance, biodiversity and resilience together affect recovery time (Hogan et al., 2020). Higher levels of biodiversity are conducive to early recovery of the ecosystem.

4.4. Limitations and outlook

This study discussed the differences in the phenological response of forests with different structures to a hurricane. We speculate that site-level phenological differences are due to the different sources of ecosystem LAI during spring green-up phase, which resulted in the plant growth rate and productivity development rate not being synchronized after mid-spring. Although total leaf area has been determined, due to data limitations, we cannot partition LAI into canopy versus understory, and therefore this assertion cannot be affirmed. To build upon this foundational research we propose that future studies use phenological cameras in both the understory and above the canopy to determine specific timing of green-up for the components of the ecosystem and how this affects the growth dynamics of both the understory and canopy. We also see this study as foundational, in that it encompasses only three years of data. Therefore, our understanding of recovery is short-term and longer periods of observation must continue.

5. Conclusion

This study explored the ecosystem-scale phenological processes of two subtropical longleaf pine forest sites with different soil water-holding capacities over three years (2017–2019), encompassing the

years before, during, and after hurricane using EC, RS, and LiDAR technology. Our results showed that hurricane caused the study sites to lose up to 30% of their LAI and up to 1.3 m in forest canopy height. The impact of the hurricane on the phenological process of longleaf pine forests in the storm year was mainly manifested in the advance of EOS, resulting in a shortening of the length of the growing season. After the hurricane, the length of the following spring recovery period was significantly longer. In this process, forest structure drove the recovery of ecosystem physiological function, and we found that there was a lag period between plant growth rate and ecosystem productivity recovery rate. This study sets the foundation for further research on the phenology of forested ecosystems impacted by hurricanes, which are forecasted to increase with changing climate.

CRediT authorship contribution statement

Conceptualization, Y.G. and G.S.; methodology, Y.G.; software, Y.G.; formal analysis, Y.G.; investigation, G.S. and G.K.; data curation, S.W. and G.K.; writing—original draft preparation, Y.G., GS and C.S.; writing—review and editing, Y.G., Y.Z., C.S., S.W, G.K. and G.S.; supervision, G.S. and C.S.; project administration, G.S.; funding acquisition, G.S. All authors have read and agreed to the published version of the manuscript.

Funding

Y.G. was funded by the Priority Academic Program Development of Jiangsu Higher Education Institutions (PAPD). C.L.S. and G.S. acknowledge support from the U.S. National Science Foundation (DEB EF-1241881). C.L.S. also acknowledges support from the U.S. National Science Foundation (DEB EF-1702029).

Declaration of competing interest

The authors declare that they have no known competing financial interests or personal relationships that could have appeared to influence the work reported in this paper.

Acknowledgements

Y.G. and Y.Z. were funded by the National Key Research and Development Program of China (No. 2016YFC0502704) and the Priority Academic Program Development of Jiangsu Higher Education Institutions (PAPD). C.S. and G.S. acknowledge support from the U.S. National Science Foundation (DEB EF-1241881 and DEB-ES 1910811). C.S. also acknowledges support from the U.S. National Science Foundation (DEB EF-1702029). Lidar data was retrieved from the National Ecological Observatory Network which is a program sponsored by the National Science Foundation and operated under cooperative agreement by Battelle Memorial Institute. This material is based in part upon work supported by the National Science Foundation through the NEON Program.

Appendix A. Supplementary data

Supplementary data to this article can be found online at https://doi.org/10.1016/j.scitotenv.2021.145651.

References

Angulo-Sandoval, P., Fernández-Marín, H., Zimmerman, J.K., Alde, T.M., 2004. Changes in patterns of understory leaf phenology and herbivory following hurricane damage. Biotropica 36 (1), 60–67.

Badeck, F.W., Bondeau, A., Böttcher, K., Doktor, D., Lucht, W., Schaber, J., Sitch, S., 2004. Responses of spring phenology to climate change. New Phytol. 162 (2), 295–309.

Bigelow, S.W., Looney, C.E., Cannon, J.B., 2020. Hurricane effects on climate-adaptive silviculture treatments to longleaf pine woodland in southwestern Georgia, USA. Forestry, 1–12 https://doi.org/10.1093/forestry/cpaa042.

Bonan, G.B., 1993. Importance of leaf area index and forest type when estimating photosynthesis in boreal forests. Remote Sens. Environ. 43 (3), 303–314.

Chambers, J.Q., Fisher, J.I., Zeng, H., Chapman, E.L., Baker, D.B., Hurtt, G.C., 2007. Hurricane Katrina's carbon footprint on US Gulf Coast forests. Science 318 (5853), 1107.

Chen, Z.W., 2019. Climatic Characteristics of the Northwest Pacific Tropical Cyclone and Its Response Mechanism with the Thermal Status of Ocean. (Ph.D. Dissertation). Shanghai Normal University, Shanghai, China Available at:. http://d.wanfangdata.com.cn/thesis/Y3543251.

Christensen, N.L., 1981. In: Mooney, H.A., Bonnicksen, T.M., Christensen Jr, N.L., Lotspeich, F.B., Reiners, W.A. (Eds.), Fire Regimes in Southeastern Ecosystems. USDA Forest Service, Washington, DC, pp. 112–136.

Drever, C.R., Lertzman, K.P., 2003. Effects of a wide gradient of retained tree structure on understory light in coastal Douglas-fir forests. Can. J. For. Res. 33 (1), 137–146.

Enquist, C.A., Kellermann, J.L., Gerst, K.L., Miller-Rushing, A.J., 2014. Phenology research for natural resource management in the United States. Int. J. Biometeorol. 58 (4), 579–589.

Goebel, P.C., Palik, B.J., Kirkman, L.K., West, L., 1997. Field Guide: Landscape Ecosystem Types of Ichauway (Joseph W. Jones Ecological Research Center at Ichauway, Newton. Report number 97–1).

Gong, Y., Zhang, Y., 2020. Characteristics of CO_2 flux over a temperate mixed forest ecosystem and its response to air temperature. J. Northeast Forest. Univ. 48 (5), 40–44 87. 10.13759/j.cnki.dlxb.2020.05.008.

Gong, Y., Guo, Z.J., Zhang, K.D., Xu, L., Wei, Y.Y., Zhao, M., 2019. Impact of vegetation on CO_2 flux of a subtropical urban ecosystem. Acta Ecol. Sin. 39 (2), 530–541.

Gong, Y., Ji, X., Hua, Y., Zhang, Y., Li, N., 2020. Research progress of CO_2 flux in forest ecosystem based on eddy covariance technique: a review. J. Zhejiang A&F Univ. 37 (3), 593–604. https://doi.org/10.11833/j.issn.2095-0756.20190412.

Gong, Y., Staudhammer, C.L., Wiesner, S., Starr, G., Zhang, Y., 2021. Characterizing growing season length of subtropical coniferous forests with a phenological model. Forests. 12, 95. https://doi.org/10.3390/f12010095.

Gonsamo, A., Chen, J.M., Price, D.T., Kurz, W.A., Wu, C., 2012. Land surface phenology from optical satellite measurement and CO_2 eddy covariance technique. J. Geophys. Res. Biogeosci. 117 (G3), G03032.

Gonsamo, A., Chen, J.M., D'Odorico, P., 2013. Deriving land surface phenology indicators from CO_2 eddy covariance measurements. Ecol. Indic. 29, 203–207.

Gonsamo, A., Croft, H., Chen, J.M., Wu, C., Froelich, N., Staebler, R.M., 2015. Radiation contributed more than temperature to increased decadal autumn and annual carbon uptake of two eastern North America mature forests. Agric. For. Meteorol. 201, 8–16.

Gu, L., Post, W.M., Baldocchi, D., Black, T.A., Verma, S.B., Vesala, T., Wofsy, S.C., 2003. Phenology of vegetation photosynthesis. In: Schwartz, M. (Ed.), Phenology: An Integrative Environmental Science. Springer, New York, pp. 467–485.

Gu, L., Post, W.M., Baldocchi, D.D., Black, T.A., Suyker, A.E., Verma, S.B., Vasala, T., Wofsy, S.C., 2009. Characterizing the seasonal dynamics of plant community photosynthesis across a range of vegetation types. Phenology of Ecosystem Processes. Springer, New York, pp. 35–58 https://doi.org/10.1007/978-1-4419-0026-5_2.

Harrington, R.A., Fownes, J.H., Scowcroft, P.G., Vann, C.S., 1997. Impact of Hurricane Iniki on native Hawaiian *Acacia koa* forests: damage and two-year recovery. J. Trop. Ecol. 539–558.

Herbert, D.A., Fownes, J.H., Vitousek, P.M., 1999. Hurricane damage to a Hawaiian forest: nutrient supply rate affects resistance and resilience. Ecology 80 (3), 908–920.

Hogan, J.A., Feagin, R.A., Starr, G., Ross, M., Lin, T.C., O'connell, C., ... Xue, J., 2020. A research framework to integrate cross-ecosystem responses to Tropical Cyclones. BioScience 70 (6), 477–489.

Johnsen, K.H., Butnor, J.R., Kush, J.S., Schmidtling, R.C., Nelson, C.D., 2009. Hurricane Katrina winds damaged longleaf pine less than loblolly pine. South. J. Appl. For. 33 (4), 178–181.

Kenney, G., Staudhammer, C.L., Wiesner, S., Brantley, S., Bigelow, S., Starr, G., 2021. The effects of Hurricane Michael on the structure and function of longleaf pine forests. Ecology. (in review).

Kirkman, L.K., Mitchell, R.J., Helton, R.C., Drew, M.B., 2001. Productivity and species richness across an environmental gradient in a fire-dependent ecosystem. Am. J. Bot. 88 (11), 2119–2128.

Kirkman, L.K., Barnett, A., Williams, B.W., Hiers, J.K., Pokswinski, S.M., Mitchell, R.J., 2013. A dynamic reference model: a framework for assessing biodiversity restoration goals in a fire-dependent ecosystem. Ecol. Appl. 23 (7), 1574–1587.

Kong, D., Zhang, Y., Wang, D., Chen, J., Gu, X., 2020. Photoperiod explains the asynchronization between vegetation carbon phenology and vegetation greenness phenology. J. Geophys. Res. Biogeosci. 125 (8), e2020JG005636.

Krausse, K., Goulden, T., 2015. NEON L0-TO-L1 Discrete-return LiDAR Algorithm Theoretical Basis Document (ATBD). The National Ecological Observatory Network Available at:. https://data.neonscience.org/.

Landsberg, J.J., Waring, R.H., 1997. A generalised model of forest productivity using simplified concepts of radiation-use efficiency, carbon balance and partitioning. For. Ecol. Manag. 95 (3), 209–228.

Lenth, R.V., 2016. Least-Squares Means: R. Package lsmeans. 69 p. 33.

Li, J., Powell, T.L., Seiler, T.J., Johnson, D.P., Anderson, H.P., Bracho, R., ... Drake, B.G., 2007. Impacts of Hurricane Frances on Florida scrub-oak ecosystem processes: Defoliation, net CO_2 exchange and interactions with elevated CO_2. Global Change Biology 13 (6), 1101–1113.

Li, Y., Liu, C., Zhang, J., Yang, H., Xu, L., Wang, Q., ... He, N., 2018. Variation in leaf chlorophyll concentration from tropical to cold-temperate forests: association with gross primary productivity. Ecological Indicators 85, 383–389.

Lindroth, A., Lagergren, F., Aurela, M., Bjarnadottir, B., Christensen, T., Dellwik, E., Grelle, A., Ibrom, A., Johansson, T., Lankreijer, H., Launiainen, D., Laurila, T., Mölder, M., Nikinmaa, E., Pilegaard, K., Sigurdsson, B.D., Vesala, T., 2008. Leaf area index is the principal scaling parameter forboth gross photosynthesis and ecosystem respiration

of Northern deciduous and coniferous forests. Tellus B Chem. Phys. Meteorol. 60 (2), 129–142.
Lloyd, J., Taylor, J.A., 1994. On the temperature dependence of soil respiration. Funct. Ecol. 8 (3), 315–323.
Ma, S., Eichelmann, E., Wolf, S., Rey-Sanchez, C., Baldocchi, D.D., 2020. Transpiration and evaporation in a Californian oak-grass savanna: field measurements and partitioning model results. Agric. For. Meteorol. 295, 108204. https://doi.org/10.1016/j.agrformet.2020.108204.
McGuire, J.P., Mitchell, R.J., Moser, E.B., Pecot, S.D., Gjerstad, D.H., Hedman, C.W., 2001. Gaps in a gappy forest: plant resources, longleaf pine regeneration, and understory response to tree removal in longleaf pine savannas. Can. J. For. Res. 31 (5), 765–778.
National Ecological Observatory Network, 2020. Data Product DP1.30003.001, Discrete Return LiDAR Point Cloud (Provisional data downloaded from http://data.neonscience.org on June 8, 2020. Battelle, Boulder, CO, USA NEON. 2020).
NCDC, 2011. Monthly Station Normals of Temperature, Precipitation, and Heating and Cooling Degree Days 1981–2010. National Climatic Data center, Asheville, NC.
Niu, S., Fu, Y., Gu, L., Luo, Y., 2013. Temperature sensitivity of canopy photosynthesis phenology in northern ecosystems. Phenology: An Integrative Environmental Science. Springer, Dordrecht, pp. 503–519.
Ostertag, R., Silver, W.L., Lugo, A.E., 2005. Factors affecting mortality and resistance to damage following hurricanes in a rehabilitated subtropical moist forest. Biotropica 37 (1), 16–24.
Pinheiro, J., Bates, D., DebRoy, S., Sarkar, D., 2014. R Core Team (2014) nlme: Linear and Nonlinear Mixed Effects Models. R package version 3.1-117. Available at:. http://cran.r-project.org/package=nlme.
R Core Team, 2013. R: A Language and Environment for Statistical Computing.
Renton, K., Salinas-Melgoza, A., Rueda-Hernández, R., Vázquez-Reyes, L.D., 2018. Differential resilience to extreme climate events of tree phenology and cavity resources in tropical dry forest: cascading effects on a threatened species. For. Ecol. Manag. 426, 164–175.
Rosati, A., Wolz, K.J., Murphy, L., Ponti, L., Jose, S., 2020. Modeling light below tree canopies overestimates net photosynthesis and radiation use efficiency in understory crops by averaging light in space and time. Agric. For. Meteorol. 284, 107892.
Starr, G., Staudhammer, C.L., Loescher, H.W., Mitchell, R., Whelan, A., Hiers, J.K., O'Brien, J.J., 2015. Time series analysis of forest carbon dynamics: recovery of *Pinus palustris* physiology following a prescribed fire. New For. 46 (1), 63–90.
Starr, G., Staudhammer, C.L., Wiesner, S., Kunwor, S., Loescher, H.W., Baron, A.F., Whelan, A., Mitchell, R.J., Boring, L., 2016. Carbon dynamics of *Pinus palustris* ecosystems following drought. Forests 7 (5), 98.
Tanner, E.V.J., Kapos, V., Healey, J.R., 1991. Hurricane effects on forest ecosystems in the Caribbean. Biotropica 23 (4a), 513–521.
Way, A.G., 2006. Burned to be wild: Herbert Stoddard and the roots of ecological conservation in the 2019southern longleaf pine forest. Environ. Hist. 11, 500–526.
Whelan, A., Mitchell, R., Staudhammer, C., Starr, G., 2013. Cyclic occurrence of fire and its role in carbon dynamics along an edaphic moisture gradient in longleaf pine ecosystems. PLoS One 8 (1), e54045.
Wiesner, S., Staudhammer, C.L., Loescher, H.W., Baron-Lopez, A., Boring, L.R., Mitchell, R.J., Starr, G., 2018. Interactions among abiotic drivers, disturbance and gross ecosystem carbon exchange on soil respiration from subtropical pine savannas. Ecosystems 21 (8), 1639–1658.
Wiesner, S., Staudhammer, C.L., Javaheri, C.L., Hiers, J.K., Boring, L.R., Mitchell, R.J., Starr, G., 2019. The role of understory phenology and productivity in the carbon dynamics of longleaf pine savannas. Ecosphere 10 (4), e02675.
Wiesner, S., Stoy, P.C., Staudhammer, C.L., Starr, G., 2020. Using metabolic energy density metrics to understand differences in ecosystem function during drought. J. Geophys. Res. Biogeosci. 125 (3), e2019JG005335.
Yang, L., Noormets, A., 2020. Standardized flux seasonality metrics: a companion dataset for FLUXNET annual product. Earth Syst. Sci. Data Discuss., 1–22 https://doi.org/10.5194/essd-2020-58.
Yun, H., Wang, J., Zhao, Q., Li, Y., 2013. Seasonal variability in leaf area index and canopy gap fraction of *Catalpa bungei*. J. Nanjing Forest. Univ. (Nat. Sci. Edit.) 37 (2), 59–64. https://doi.org/10.3969/j.issn.1000-2006.2013.02.011.
Zhang, X., Friedl, M.A., Schaaf, C.B., Strahler, A.H., Hodges, J.C., Gao, F., Reed, B.C., Huete, A., 2003. Monitoring vegetation phenology using MODIS. Remote Sens. Environ. 84 (3), 471–475.
Zhang, W., Villarini, G., Vecchi, G.A., Smith, J.A., 2018. Urbanization exacerbated the rainfall and flooding caused by hurricane Harvey in Houston. Nature 563 (7731), 384–388.
Zhang, W., Yu, G., Chen, Z., Zhang, L., Wang, Q., Zhang, Y., ... Li, Y., 2020. Attribute parameter characterized the seasonal variation of gross primary productivity (αGPP): Spatiotemporal variation and influencing factors. Agricultural and Forest Meteorology 280, 107774.
Zhou, Y., 2019. Asymmetric behavior of vegetation seasonal growth and the climatic cause: evidence from long-term NDVI dataset in northeast China. Remote Sens. 11 (18), 2107.